Proceedings of the 2000 IEEE International Conference on Robotics and Automation, San Francisco, CA, April 24-28, pp. 2064-2069

Precision-calibration of Fiber-optics Gyroscopes for Mobile Robot Navigation

by
Lauro Ojeda, Hakyoung Chung, and Johann Borenstein*
The University of Michigan
Dept. of Mechanical Engineering and Applied Mechanics
lojeda@umich.edu; chy@duck.snut.ac.kr; johannb@umich.edu

ABSTRACT

Fiber-optics gyroscopes ("gyros") are gaining importance as a means for improving dead-reckoning accuracy in mobile robots. In the past, the relatively high drift rate of moderately priced gyros presented the foremost technical limitation of these devices.

More recently, fiber-optics gyros with very low drift rates have become available and affordable. Because of their low drift rate attention is warranted to sources of errors that were previously considered as of secondary importance. In the KVH E-Core RD2100 gyros that were examined at our lab we found that the non-linearity of the scale-factor and temperature dependency caused significant errors. A calibration method, described in this paper, reduces the resulting errors by one order of magnitude.

1. INTRODUCTION

Dead-reckoning is widely used in mobile robot navigation because the method is self-contained and always capable of providing the robot with an estimate of its position. Odometry is the most frequently used component in a dead-reckoning system, but increasingly gyroscopes are being used as well. However, with dead-reckoning the position and heading errors increase without bound. Filtering scheme such as Kalman filter can be utilized to reduce these errors [Park et al., 1996; Barshan, B., and Durrant-Whyte, H. F., 1995], but an observability analysis shows that the states related to the position and heading are unobservable. That means that dead-reckoning system has the inevitable characteristics of divergence [Park et al., 1998]. Therefore errors, especially deterministic errors of dead-reckoning sensors, should be reduced before they affect the navigation system.

The University of Michigan's Mobile Robotics Lab has been working with fiber-optics gyroscopes (in short: "gyros") for several years [Borenstein et al., 1996; Borenstein, 1998]. As a result we identified the need for accurate calibration procedures in order to improve measurement accuracy. This paper describes the motivation and technique for a calibration procedure that improves measurement accuracy by one order of magnitude.

One key concern with the use of gyros as a means for improving dead-reckoning in mobile robots is the inherent bias drift. Bias drift is the slowly changing error in measuring the rate-of-rotation. For example, a stationary gyro should output readings of $\omega_g = 0.00$ °/s. In practice, however, the reading will differ from that value due to bias drift. For dead-reckoning purposes it is necessary to perform numeric integration of the output readings, ω_g, in order to determine relative orientation. Due to this integration any small constant or near-constant error (as opposed to noise) will accumulate and grow without bound, resulting in ever-increasing orientation errors.

Until just a few years ago all but the highest-grade mechanical gyroscopes had large bias drift rates. These rates would accumulate several degrees of orientation error after, say, one minute. Such large error rates made it impractical to use suitably priced gyros on mobile robots.

This situation changed with the reduction in cost of commercially available fiber-optics gyros. For example, the KVH E-Core RD2100 gyro [KVH], which was the model used in our experiments, costs about $2,000 and its drift rate is specified as (at most) 0.002°/s = 0.12°/min = 7.2°/hr (see Table I). With these specifications it is feasible to run a mission of, say, 10 minutes duration, while incurring an orientation error of at most 1.2°

However, with the reduction of bias drift errors other measurement errors gain in relative significance. Most notable among these hitherto secondary error are (1) the *nonlinearity of the scale factor* and (2) the *susceptibility of the sensor to changes in ambient temperature*. These two errors can be reduced substantially by performing an individual calibration for each gyro.

This paper presents a calibration procedure developed at our lab specifically for the KVH E-Core RD2100, which was previously made by Andrews Corp. under the

Table I: Technical specifications for the E-Core RD2100 fiber-optics gyroscope. (Courtesy of [KVH])

Performance		**RD2100**
Input Rate (max)	± °/sec	100
Resolution	°/sec	0.004
Scale factor	°/bit	0.000305
Nonlinearity	%, rms	0.5
Full Temp	%, p-p	2
Bias Stability		
Constant Temp	°/sec, 1	0.002
Full Temp	°/sec, p-p	0.2
Repeatability	°/sec, p-p	0.002
Angle Rand. Walk	(°/hr)/ Hz	5
	°/ hr	0.08
Bandwidth (3 dB)	45° phase shift	100

name *Autogyro*. Specifications for the RD2100, as published by the manufacturer, are shown in Table I. As will be seen, consistent improvements of one order of magnitude in accuracy over a wide range of operating conditions are achieved by applying our calibration procedure.

2. Static Bias Drift Calibration

A common compensation procedure for static bias drift (see Figure 1) is to collect several samples (for, say, 10-20 seconds) with the gyro stationary and *immediately prior to every mission*.

Specifically, this is done by computing

$$w_s = \frac{1}{n}\sum_{i=1}^{n} w_{g,i} \qquad (1)$$

where

ω_s - static bias drift

n - total number of samples (n = 100 for a 10-second sample with the RD2100)

During the immediately following mission, ω_s is subtracted from subsequent measurements ω_g. Since the static bias drift is small for the RD2100, this technique will assure that errors due to static bias drift will be less than about one degree for subsequent missions of fewer than 10 minutes of duration. Note that ω_s also includes the rate-of-rotation component introduced by the earth's rotation. However, this simple method does not correct the errors due to the non-linearity in the scale factor and temperature, discussed next.

3. Calibration

The procedure discussed in this section aims at finding a mathematical model for representing the error of the gyro due to the changes in the temperature, static bias drift error, and non-linearity in the scale factor.

Our basic approach is to rotate the gyro at different, accurately controlled rates-of-rotation while maintaining different temperatures. In order to provide accurate rotation the gyro is mounted on an Arrick Robotics stepper motor-driven 4:1 reduction gear that serves as a rotary table [ARRICK] (see Figure 2). While this rotary table is very inexpensive, precision timing routines and control software for stepper motors developed at our lab allow for accurate rates-of-rotation to be obtained. The rotary table can rotate at rates of ±100°/s, which is the maximum input rotation rate of the RD2100.

In order to calculate the effect of the change in temperature on the gyro's output, one should be able to change the ambient temperature through the range of temperatures the gyro will encounter under actual working conditions. However, this goal was not implemented in our work, due to cost constraints (i.e., requirement for an environmental chamber).

In our work we varied the ambient temperature only within the rather limited range of 25° - 45°. However, the method developed in this paper is, of course, applicable to calibration sessions with larger changes of temperatures.

3.1 Non-linearity of the scale factor

As mentioned above, the basic idea is to rotate the gyro at a known input rate ω, and compare this value with the measurement output of the gyro, ω_g. The difference ε between both values is the error introduced by the gyro because of the non-linearity in the scale factor.

$$e = w_g - w \qquad (2)$$

The same procedure has to be repeated at different speeds trying to cover the whole range of operation of the gyro. The result of this experiment provides the error characteristic due to the non-linearity of the scale factor (see Figure 3).

The resulting error can be approximated by a third-order polynomial

$$e(w_g) = a_0 + a_1 w_g + a_2 w_g^{\,2} + a_3 w_g^{\,3} \qquad (3)$$

3.2 Effect of the changes in temperature

Up to here the procedure did not consider the effect of the temperature T, but, as Figure 4 shows, the measurement error ε varies with temperature. This relationship can be expressed in terms of a second-order polynomial

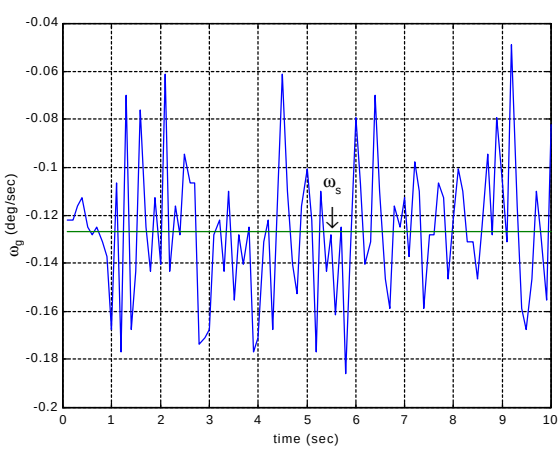

Figure 1: Output readings of the stationary gyro over a 10- seconds period. The average of these readings is the momentary static bias drift.

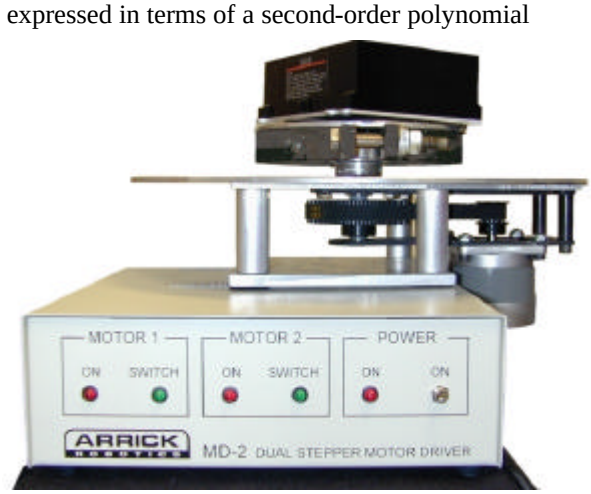

Figure 2: The KVH E-Core RD2100 mounted on the Arrick Robotics stepper motor-driven 4:1 reduction gear that served as a rotary table during experimentation.

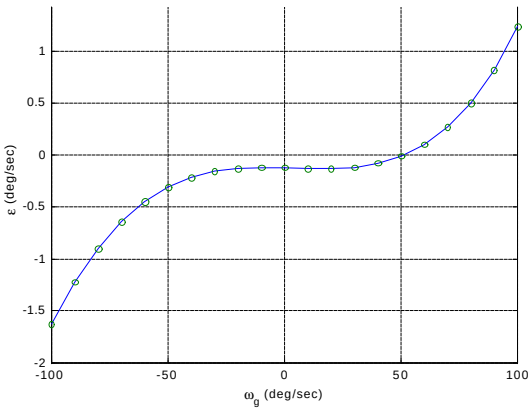

Figure 3: The error due to the non-linearity in the scale factor. The range of input rates in this and all subsequent experiments was –100°/s to +100°/s.

$$e(t) = b_0 + b_1 T + b_2 T^2 \qquad (4)$$

The parameters b_i are not constant but depend of the input rate of rotation, ω. This means that all experiments must be repeated at different temperatures to calculate the final error model or compensation function of the gyro.

We should also note that beyond the error sources considered here there are still other sources of errors. For example: angle random walk (white noise), bias instability, and magnetic sensitivity. However, the effects of these error sources are secondary.

3.3 Defining the error function

In order to determine the calibration function for the gyro, gyro data was collected under varying conditions. We will refer to the gyro data collected during rotation at a fixed rate-of-rotation and at a fixed temperature as one *data set*. Because of white noise in the gyro output and vibration introduced by the rotary table it is desirable to average the readings obtained in any one data set.

In practice this is done by defining two data vectors for each rate-of-rotation, w_i. One for the output of the gyro, ws_i, and the other for the corresponding temperatures, Ts_i.

$$ws_{gi} = \begin{bmatrix} ws_{gi1} \\ ws_{gi2} \\ . \\ . \\ ws_{gim} \end{bmatrix} \quad Ts_i = \begin{bmatrix} Ts_{i1} \\ Ts_{i2} \\ . \\ . \\ Ts_{im} \end{bmatrix} \qquad (5)$$

where m is the number of data points in a data set.

The average value of each set is then computed from

$$w_{gi} = \frac{1}{m}\sum_{j=1}^{j=m} ws_{gij}$$
$$T_i = \frac{1}{m}\sum_{j=1}^{j=m} Ts_{ij} \qquad (6)$$

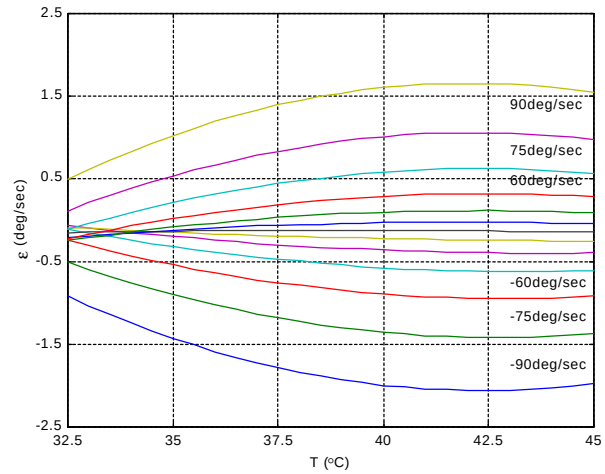

Figure 4: Gyro measurement errors due to changes in temperature at different rates-of-rotation.

The final result comprises three vectors: w, w_g, and T, all of dimension n

$$w = \begin{bmatrix} w_1 \\ w_2 \\ . \\ . \\ w_n \end{bmatrix} \quad w_g = \begin{bmatrix} w_{g1} \\ w_{g2} \\ . \\ . \\ w_{gn} \end{bmatrix} \quad \mathbf{T} = \begin{bmatrix} T_1 \\ T_2 \\ . \\ . \\ T_n \end{bmatrix} \qquad (7)$$

The difference between the output of the gyro, ω_{gi}, and the rate of rotation of the rotary table, ω_i, represents the error of the gyro ε_i at temperature T_i, (see Figure 5).

The next step is to find a mathematical model of the error ε as a function of the known variables: the output of the gyro, ω_g, and the temperature, T

$$e = f(T, w_g) \qquad (8)$$

Finding an error model from the measurements, ω_g and T, is a two-input single-output system identification problem. In order to use a general least-square algorithm for a single-input single-output system, we adopted a *Vandermonde* matrix (explained below) that reduces the problem to a single-input single-output system.

We determined the order of the polynomial function that best fits the error characteristic of the gyro by considering modeling error and computational burden. We found the best match with the error data was obtained from a polynomial function of third order with respect to the rate of rotation (p = 3) and of second order with respect to the temperature (q = 2). The general regression problem can now be formulated in a linear equation as

$$\mathbf{E} = \mathbf{VC} \qquad (9)$$

where $\mathbf{E} = [\varepsilon_1, \varepsilon_2, \ldots \varepsilon_n]^T$ is an n-dimensional output vector. $\mathbf{V}$ is an input matrix characterized by the *Vandermonde* matrix, which has a dimension of n rows and $(p+1)(q+1)$ columns. $\mathbf{C}$ is a system vector. The *Vandermonde* matrix $\mathbf{V}$ is defined as [Press et al., 1982]:

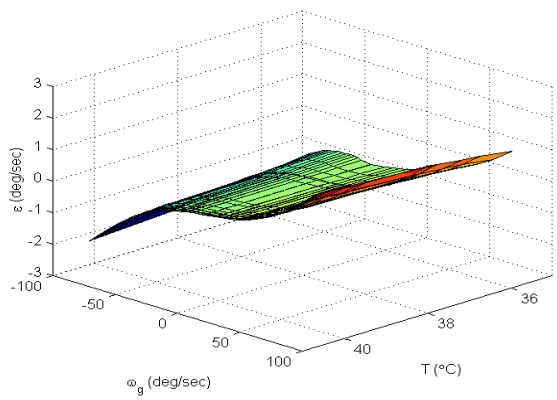

a

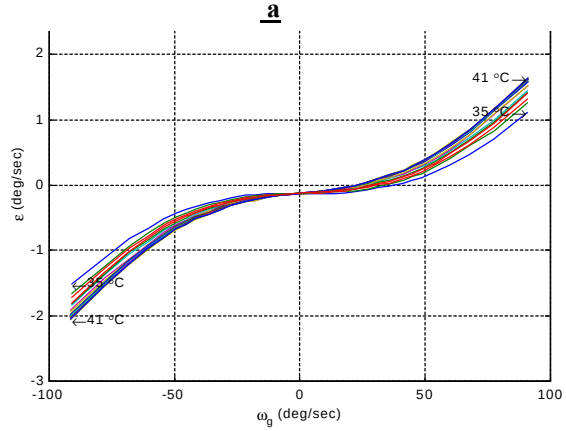

b

Figure 5: Experimental error of the gyro at different speeds and temperatures. Note that the relative small errors due to temperature variations are coincidental in this particular gyro unit.

$$V_{k,i+(j-1)p} = w_{gk}^{(p-i+1)} \otimes T_k^{(q-j+1)} \qquad (10)$$

where

$i = 1,2,\ldots, p+1$; $j = 1,2,\ldots, q+1$; $k = 1,2,\ldots, n$

The symbol "$\otimes$" represents an element-by-element multiplication of two vectors of the same dimension.

The next step is to use the *Vandermonde* matrix to calculate **C**. For a solution to exist, n must be equal to or greater than $(p+1)(q+1)$. If $n = (p+1)(q+1)$, **C** is the solution of the equation **E**= **VC** (i.e., **C** = $\mathbf{V}^{-1}$ **E**). If $n > (p+1)(q+1)$, **C** is a solution of the system **E**= **VC** in the least squares sense [Whittaker and Robinson, 1967].

For $p = 3$ and $q = 2$, the minimum n is 12, but it has to be taken at four different rates of turn and for each rate of turn at three different temperatures. For better results in practice we took readings every 10 deg/sec with the temperature varying from 25°C to 45°C approximately every 2°C, therefore $p = 11$ and $q = 11$, resulting in $n = 121$.

The resultant **C** is a $(p+1)(q+1)$-dimensional vector that can be written in matrix form as:

$$\mathbf{C} = \begin{bmatrix} C_{0,0} & C_{0,1} & C_{0,2} & C_{0,3} \\ C_{1,0} & C_{1,1} & C_{1,2} & C_{1,3} \\ C_{2,0} & C_{2,1} & C_{2,2} & C_{2,3} \end{bmatrix} \qquad (11)$$

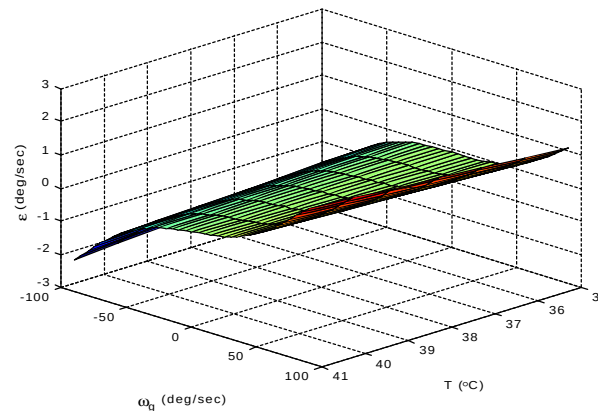

a

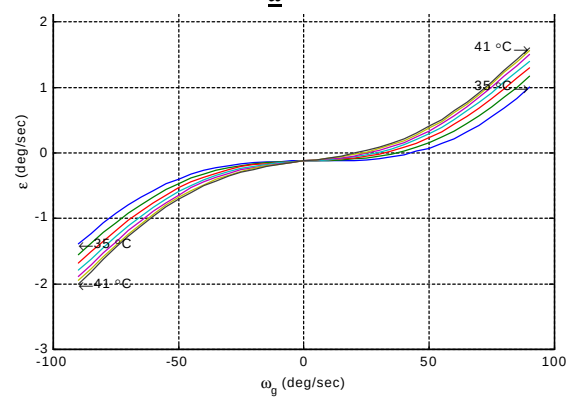

b

Figure 6: Plot of the error/compensation function $\varepsilon(\omega_g, T)$. a. 3-dimesional view. b. 2-dimensional view of a.

Using this notation, the compensation function can be expressed in such a way that, given the temperature and output of the gyro, the proper correction is calculated.

$$e(w_g, T) = \begin{bmatrix} T^2 & T & 1 \end{bmatrix} \begin{bmatrix} C_{0,0} & C_{0,1} & C_{0,2} & C_{0,3} \\ C_{1,0} & C_{1,1} & C_{1,2} & C_{1,3} \\ C_{2,0} & C_{2,1} & C_{2,2} & C_{2,3} \end{bmatrix} \begin{bmatrix} w_g^3 \\ w_g^2 \\ w_g \\ 1 \end{bmatrix} \qquad (12)$$

The error function $\varepsilon(\omega_g, T)$, shown in Figure 6, can now be used as a compensation function, simply by subtracting the appropriate value of $\varepsilon(\omega_g, T)$ from every gyro measurement ω_g.

$$w_g{*} = w_g - e(w_g, T) \qquad (13)$$

where

ω_g - Gyro reading before compensation

$\omega_g{*}$ - Compensated gyro reading

Figure 7 shows the errors of the gyro *after* correcting its output with the compensation function in Eq. 12.

4. Error Analysis for Full 360° Turns

In mobile robot applications the gyro is most likely being used to measure changes in the orientation of the platform. For this reason it is not very intuitive for the researcher to know the error of the gyro in terms of °/s. A

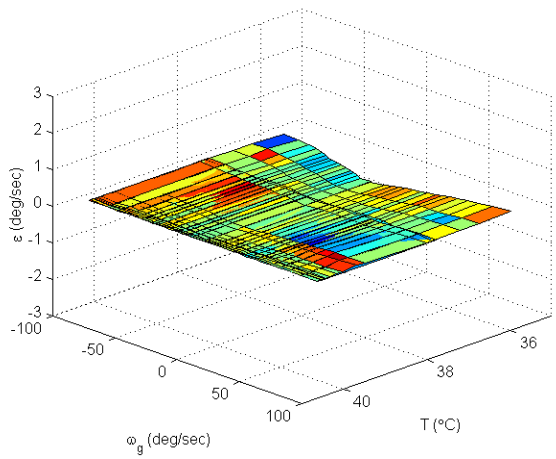

a

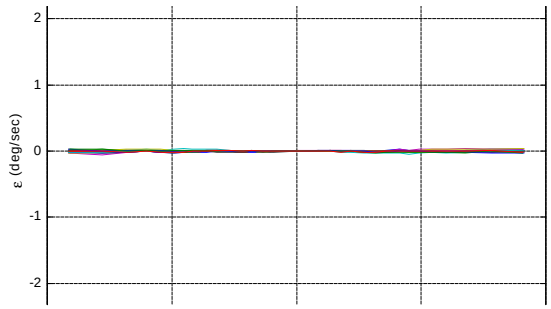

b

Figure 7: Gyro error after applying the compensation function $\varepsilon(\omega_g, T)$. a. 3-D view. b. 2-D view of multiple lines corresponding to different temperatures are plotted in b.

more intuitive measure is the error after integration (i.e., expressed in degrees), for a nominal 360° turn.

In this section we analyze gyro measurement errors in terms of degrees for a nominal 360° turn. Because numeric integration of the *native* output of the gyro is an additional source of errors, the overall error, ε_a, will be affected by all of these parameters: the rate of rotation ω_g, the temperature (T), the data output frequency of the gyro f_s and the time required to complete the full 360° turn (t). We thus rewrite Eq. (8) as

$$e_a = e(T, w_g) f_s t \qquad (14)$$

The KVH E-Core RD2100 has an RS-232 digital output that provides data every 100 ms, that is, the data output frequency f_s is 10 Hz. The rate-of-rotation of the gyro mounted on our Arrick rotary table is considered constant throughout the full 360° turn. Acceleration and deceleration at the beginning and end of the turn are neglected because the full rotational reference speed is reached within a fraction of a second.

It is important to note that in this section all plots showing errors in terms of degrees-per-360°-turn have singularities around $\omega = 0$°/s. This is because at $\omega = 0$°/s it takes infinitely long to complete the 360° turn, and, thus, the bias drift will grow without bound to an infinite error. For this reason we ran our tests at a minimum rate of rotation of $|\omega_{min}| = |\pm 5°/s|$.

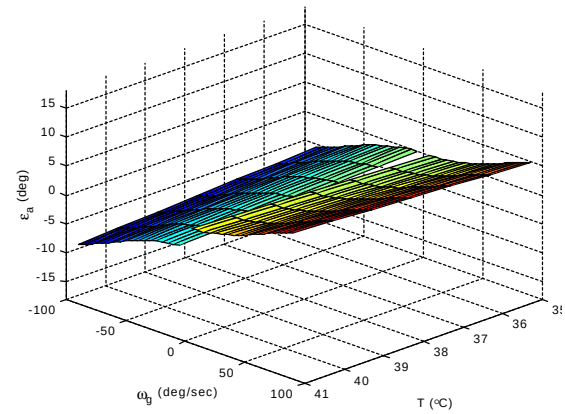

a

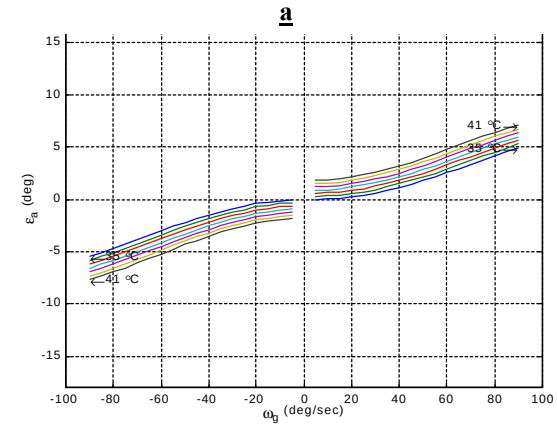

b

Figure 8: Experimental results of the accumulated error for full 360° turns, when only static bias drift compensation is applied. a. 3-D view. b. 2-D view of a.

To date we have calibrated five gyros using our procedure, and have found that each gyroscope present a different error characteristic. We have used two of them in our robots for almost one year, and so far neither of them required recalibration. However when the gyro is powered for extended periods, we observed that errors increased moderately. Further experiments revealed that this effect was directly related to the static bias drift.

The static bias drift, it is computed as

$$w_s^* = \frac{1}{n}\sum_{i=1}^{n}\left(w_{g,i} - e(w_{g,i}, T_i)\right) \qquad (15)$$

where

ω^*_s - average static bias drift computed *with* our compensation function

The combined compensation applied to all subsequent gyro readings for a mission is thus

$$w_g^{**} = w_g - e(w_g, T) - w_s^* \qquad (16)$$

The graph in Figure 8 shows the errors for a gyro after using the simple static-bias compensation discussed in Section 2, but not the comprehensive calibration function discussed in Section 3.

As is evident from Figure 8, the errors for a 360° turn can be quite substantial when only the simple static bias drift compensation of Section 2 is used prior to each run. In contrast, when our compensation function is used, errors are much smaller, as evident in Figure 9.

5. CONCLUSIONS

This paper presents experimental results of a calibration procedure for fiber-optics gyroscopes. This method has been developed and tested with five identical units of the KVH E-Core RD2100.

Our method measures errors for static bias drift, nonlinearity in the scale factor, and changes in temperature. A temperature-varying third-order polynomial function is defined based on this experimental data. This function can then be used for error compensation of subsequent readings of the gyro. Experimental data shows that the final error after compensation was reduced to less than 2% over all operating conditions.

Application of our compensation method was found to improve the overall accuracy of the five gyros tested at our lab by one order of magnitude. Indeed, these results have let us to conclude that a calibrated fiber-optics gyroscope is the single, most effect sensor modality for mobile robot dead-reckoning systems.

Acknowledgements

This work was funded by DARPA under Award No DAAE07-98-C-L029 and by DOE under Award No. DE-FG04-86NE37969.

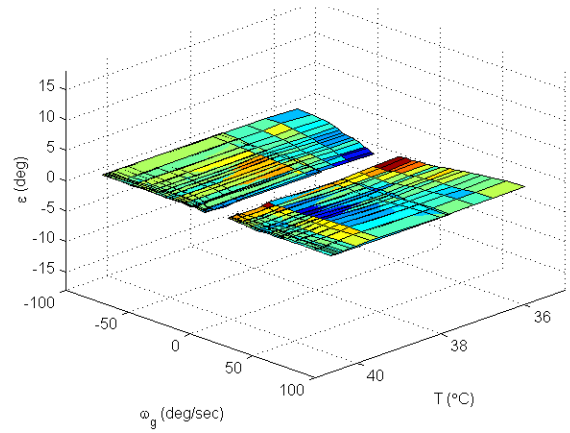

a

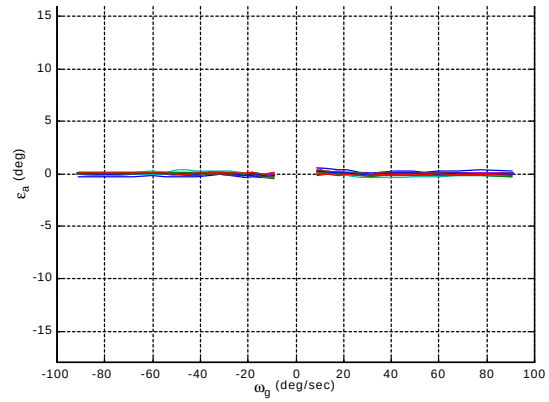

b

Figure 9: Experimental results of the accumulated error for full 360° turns, after the compensation function has been applied. a. 3-D view. b. 2-D view of a. Multiple lines corresponding to different temperatures are plotted in b.

6. REFERENCES

ARRICK, P.O. Box 1574, Hurst, Texas, 76053 USA, http://www.robotics.com/resource.html

Barshan, B., and Durrant-Whyte, H. F., 1995, "Inertial Navigation Systems Mobile Robots." *IEEE Transaction on Robotics and Automation*, June, pp. 328-342.

Borenstein, J., Everett, B., and Feng, L., 1996, "*Navigating Mobile Robots: Systems and Techniques."* A. K. Peters, Ltd., Wellesley, MA, ISBN 1-56881-058-X, Publication Date: February 1996.

Borenstein, J., 1998, "Experimental Evaluation of a Fiber Optics Gyroscope for Improving Dead-reckoning Accuracy in Mobile Robots." *1998 IEEE Int. Conf. on Robotics and Automation.* Leuven, Belgium, May 16-21, pp. 3456-3461.

Bennett, S. M., Dyott, R., Allen, D., Brunner, J., Kidwell, R. and Miller, R., 1998, "Fiber Optic Rate Gyros as Replacements for Mechanical Gyros." *American Institute of Aeronautics and Astronautics*, AIAA-98-4401, Boston, MA, Aug 10-12, pp. 1315-1321.

KVH, 8412 W. 185th St., Tinley Park, IL 60477, USA, http://KVH.com.

Park, K., Chung, H., and Lee, J., 1996, "Dead Reckoning Navigation of a Mobile Robot Using the Indirect Kalman Filter." *Proc. of the IEEE/SICE/RSJ Int. Conf. on Multisensor Fusion and Integration for Intelligent Systems*, Washington D.C. USA, Dec. 8-11, pp. 132-138.

Park, K., Chung, H., and Lee, J., 1998, "Dead Reckoning Navigation for Autonomous Mobile Robots." *Proceeding of Intelligent Autonomous Vehicle*, Madrid, Spain, March 25-28, pp. 441-446.

Press, W. H., Flannery, B. P., Teukolsky, S. A., and Vetterling, W. T. 1982, "*Numerical Recipes in FORTRAN: The Art of Scientific Computing*." 2nd ed. Cambridge, England: Cambridge Univ. Press, pp. 82-89.

Whittaker, E. T. and Robinson, G., 1967, "*The Calculus of Observations: A Treatise on Numerical Mathematics*." 4th ed. New York, Dover, pp. 209-265.